Princeton Plasma Physics Laboratory

PPPL- 4430

PPPL- 4430

Electron Gyro-scale Fluctuation Measurements in National Spherical Torus Experiment H-mode Plasmas

D.R. Smith, S.M. Kaye, W. Lee, E. Mazzucato, H.K. Park, R.E. Bell, C.W. Domier, B.P. LeBlanc, F.M. Levinton, N.C. Luhmann, Jr., J.E. Menard, and H. Yuh

August, 2009

PPPL PRINCETON PLASMA PHYSICS LABORATORY

Prepared for the U.S. Department of Energy under Contract DE-AC02-09CH11466.

Princeton Plasma Physics Laboratory
Report Disclaimers

Full Legal Disclaimer

Trademark Disclaimer

PPPL Report Availability

Princeton Plasma Physics Laboratory:

http://www.pppl.gov/techreports.cfm

Office of Scientific and Technical Information (OSTI):

http://www.osti.gov/bridge

Related Links:

U.S. Department of Energy

Office of Scientific and Technical Information

Fusion Links

Electron gyro-scale fluctuation measurements in National Spherical Torus Experiment H-mode plasmas*

D. R. Smith[1†,‡] S. M. Kaye[1], W. Lee[2], E. Mazzucato[1],
H. K. Park[2], R. E. Bell[1], C. W. Domier[3], B. P. LeBlanc[1],
F. M. Levinton[4], N. C. Luhmann, Jr.[3], J. E. Menard[1], and H. Yuh[4]

[1]*Princeton Plasma Physics Laboratory, Princeton, NJ 08543, USA*

[2]*Pohang University of Science and Technology, Pohang 790-784, Korea*

[3]*Department of Applied Science, University of California at Davis, Davis, CA 95616, USA*

[4]*Nova Photonics, Inc., Princeton, NJ 08540, USA*

(Dated: July 22, 2009)

Abstract

A collective scattering system has measured electron gyro-scale fluctuations in National Spherical Torus Experiment (NSTX) H-mode plasmas to investigate electron temperature gradient (ETG) turbulence. Observations and results pertaining to fluctuation measurements in ETG-stable regimes, the toroidal field scaling of fluctuation amplitudes, the relation between between fluctuation amplitudes and transport quantities, and fluctuation magnitudes and k-spectra are presented. Collectively, the measurements provide insight and guidance for understanding ETG turbulence and anomalous electron thermal transport.

PACS numbers: 52.35.Ra, 52.55.Fa, 52.65.Tt, 52.70.Gw

Keywords: NSTX, ETG turbulence, collective scattering

* Paper YI2 5, Bull. Am. Phys. Soc. **53** (2008)

† Invited speaker.

‡Electronic address: drsmith@pppl.gov; Present address: Department of Engineering Physics, University of Wisconsin-Madison, Madison, WI 53706, USA

I. INTRODUCTION

Anomalous electron thermal transport in magnetically-confined plasma hinders efforts to achieve feasible magnetic fusion energy. Nonlinear gyrokinetic simulations indicate electron temperature gradient (ETG) turbulence can generate experimentally-relevant electron thermal transport for certain plasma regimes [1, 2]. ETG turbulence occurs on the electron gyro-scale with $k_\perp \rho_e \lesssim 1$, where $k_\perp$ is the fluctuation wavenumber perpendicular to the magnetic field and ρ_e is the electron gyro-radius. Nonlinear gyrokinetic simulations predict ETG turbulence can saturate at higher normalized amplitude and generate greater normalized transport than ion temperature gradient (ITG) turbulence [3–5]. Secondary instabilities and zonal flows regulate drift wave instabilities, like the ETG and ITG modes. The ion response for ETG turbulence, however, weakens ETG secondary instabilities in relation to ITG turbulence. To test predictions of ETG turbulence from nonlinear gyrokinetic simulations, fluctuation measurements on the electron gyro-scale are needed.

The National Spherical Torus Experiment (NSTX) [6, 7] is a low-aspect-ratio tokamak well suited for investigating ETG turbulence and electron thermal transport. NSTX H-mode plasmas with neutral beam injection (NBI) exhibit ion thermal transport at or near neoclassical levels, and electron thermal transport is always anomalous and dominant in most cases. Toroidal rotation from NBI generates large equilibrium $E \times B$ flow shear rates that typically exceed ITG and trapped-electron mode (TEM) growth rates. Neoclassical ion thermal transport in NSTX H-mode plasmas with NBI is attributed to the inferred flow shear suppression of ITG and TEM turbulence. The ETG mode, on the other hand, can be linearly unstable in NSTX plasmas with growth rates exceeding $E \times B$ flow shear rates. Accordingly, NSTX is well suited for investigating ETG turbulence.

To investigate ETG turbulence, a collective scattering system was installed on NSTX to measure electron gyro-scale fluctuations [8–10]. The NSTX collective scattering system simultaneously measures up to five distinct wavenumbers with $k_\perp \rho_e \lesssim 0.6$. The scattering system is configured for tangential measurements, so measured wave vectors are primarily radial. The radial localization and k-space resolution are $\Delta R \approx \pm 3$ cm and $\Delta k_\perp \approx 1$ cm^{-1}, respectively, and steerable optics can position the scattering volume from the magnetic axis to the last-closed flux surface.

Past collective scattering measurements in NSTX revealed electron gyro-scale fluctuations

in L-mode plasmas with high-harmonic fast-wave heating [11, 12]. Enhanced fluctuations were observed when the local electron temperature gradient exceeded the ETG linear critical gradient, and the enhanced fluctuations propagated with a component in the electron diamagnetic direction. In H-mode plasmas with NBI heating, scattering measurements revealed electron gyro-scale fluctuations when the electron temperature gradient was marginally stable with respect to the ETG linear critical gradient, and fluctuation amplitudes decreased when the equilibrium $E \times B$ shear rate exceeded ETG linear growth rates [13]. In this Paper, we investigate several additional topics including fluctuation measurements in ETG-stable regimes in Section II, the toroidal field scaling of fluctuation amplitudes in Section III, the relationship between fluctuation amplitudes and transport quantities in Section IV, and fluctuation magnitudes and k-spectra in Section V [14]. Finally, Section VI presents a summary of results.

II. FLUCTUATION MEASUREMENTS IN ETG-STABLE REGIONS

This Section presents electron gyro-scale fluctuation measurements in H-mode discharges near the magnetic axis where the electron temperature gradient is small [14]. Electron gyro-scale fluctuations associated with ETG turbulence should not be observed if the electron temperature gradient is less than the ETG critical gradient. Additionally, the region near the magnetic axis in H-mode plasmas ($r/a \lesssim 0.2$) exhibits small equilibrium $E \times B$ shear rates, similar to the L-mode plasmas with HHFW heating in Refs. 11 and 12.

Figure 1 shows discharge profiles for a 4.5 kG H-mode plasma with fluctuation measurements at $R = 113 \pm 2$ cm and $r/a = 0.1$–0.2. The Mirnov signal is approximately steady-state for the period 340–500 ms, and the neutron signal does not show fast-ion loss events. Figure 2 shows fluctuation measurements and ray tracing calculations at $R = 113 \pm 2$ cm and $r/a = 0.1$–0.2. Enhanced fluctuations occur briefly at 330 ms and persist after 450 ms. In Figure 2, positive frequency corresponds to fluctuations that propagate with a wave vector component in the ion drift direction in the *lab* frame. Toroidal rotation induces a Doppler shift toward the ion direction such that peak amplitudes in Figure 2 correspond to fluctuations that propagate with a wave vector component in the electron drift direction in the *plasma* frame. Accordingly, the wavenumber range and propagation direction of the measured fluctuations in Figure 2 are consistent with ETG turbulence. Note that ray tracing

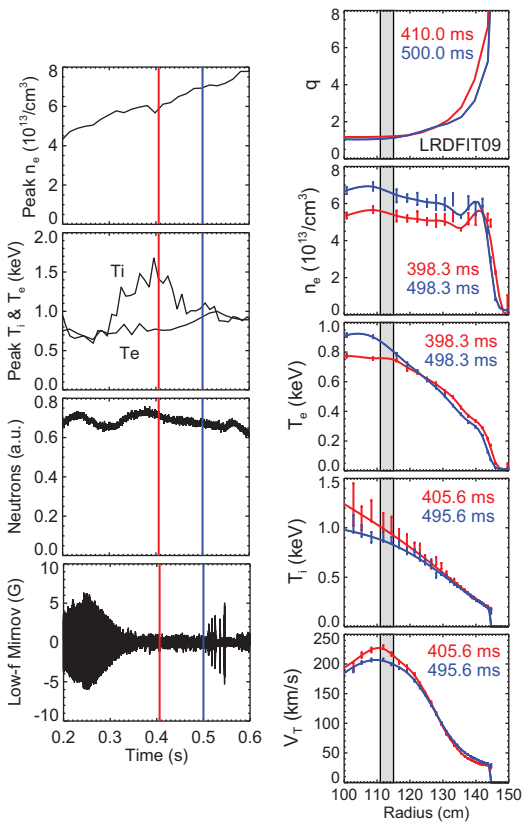

FIG. 1: Discharge 124887 with deuterium gas, $B_T = 4.5$ kG, $I_p = 700$ kA, and 4 MW of NBI heating. Fluctuation measurements were obtained at $R = 113 \pm 2$ cm (gray box).

calculations indicate the length of the scattering volume along the probe beam in Figure 2 is less than 1 cm. The nearly toroidal magnetic field near the magnetic axis generates the narrow selectivity function [15, 16]. The peak in the instrument selectivity function, however, varies by about 3 cm along the probe beam for rays within the probe beam antenna pattern. A realistic calculation of the scattering volume length near the magnetic axis may require a full-wave calculation. In addition, spectral features in the range 1–2 MHz in Figure 2 are consistent with Doppler-shifted fluctuations with calculated toroidal wavenumbers, so the observed fluctuations are consistent with high-k fluctuations.

Figure 3 shows ETG critical gradients and growth rates for measurements in Figures 1 and 2. Note that the $E \times B$ shear rate is relatively low at about 20–30 kHz. The brief period of enhanced fluctuations at 330 ms occurs when the electron temperature gradient briefly exceeds the ETG critical gradient. The increase in fluctuation amplitudes after 450 ms, however, occurs during a period of ETG stability. The measurements indicate

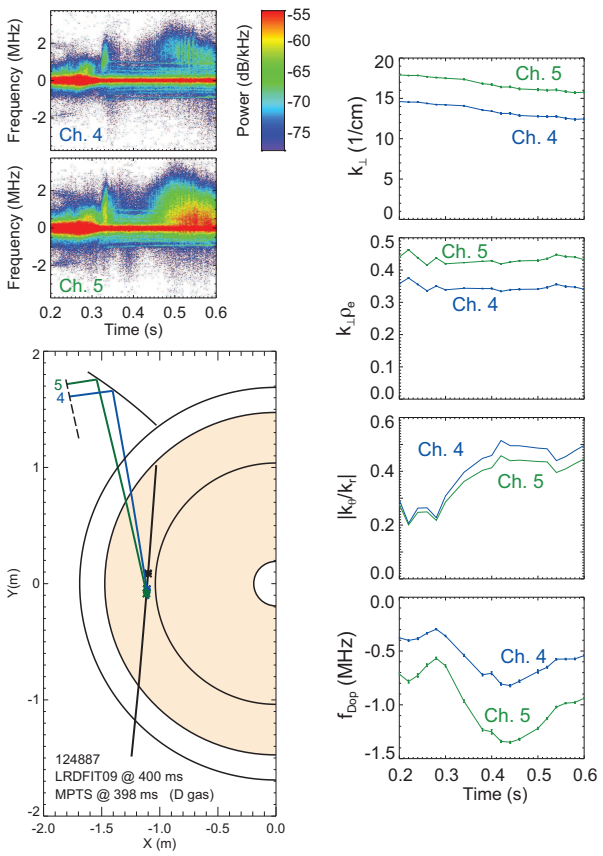

FIG. 2: Fluctuation measurements and ray tracing calculations for discharge 124887 at $R = 113 \pm 2$ cm in Figure 1.

electron gyro-scale fluctuations are present during a period of ETG linear stability. The observations are inconsistent with linear stability theory for ETG turbulence and suggest an additional turbulence mechanism is present, such as high-k micro-tearing modes or an ITG/TEM high-k "tail" [2, 17].

Figure 4 shows discharge profiles for a 5.5 kG H-mode plasma with fluctuation measurements at $R = 113 \pm 2$ cm and $r/a = 0.1$–0.2. The low frequency Mirnov signal is steady-state after 400 ms, and the neutron signal indicates fast-ion losses are absent. Figure 5 shows fluctuation measurements and ray tracing calculations at $R = 113 \pm 2$ cm and $r/a = 0.1$–0.2. Enhanced fluctuations occur between 400 and 450 ms and after 600 ms. In Figure 5, positive frequency corresponds to fluctuations that propagate with a wave vector component in the ion drift direction in the *lab* frame. Toroidal rotation induces a Doppler shift toward the ion direction such that peak amplitudes in Figure 5 correspond to fluctuations that propagate with a wave vector component in the electron drift direction in the *plasma* frame.

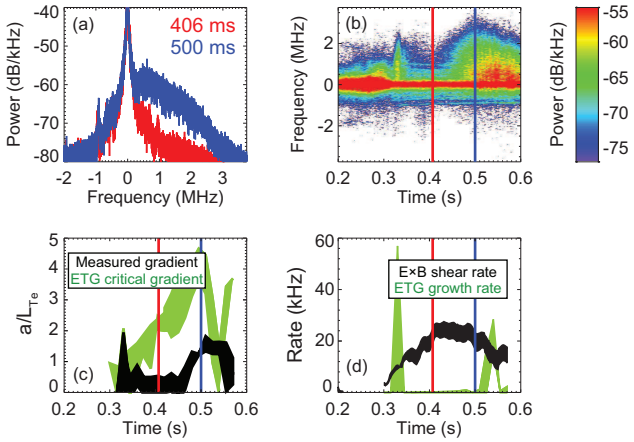

FIG. 3: (a and b) Fluctuation measurements for Ch. 5, (c) electron temperature gradient and ETG linear critical gradient, and (d) $E \times B$ shear rate and ETG linear growth rate for data in Figures 1 and 2.

Accordingly, the wavenumber range and propagation direction of the observed fluctuations are consistent with ETG turbulence. As in Figure 2, the scattering volume length along the probe beam in Figure 5 is less than 1 cm. However, the peak in the selectivity function varies by about 3 cm along the probe beam for rays within the probe beam antenna pattern, and the observed fluctuations are consistent with Doppler-shifted high-k fluctuations. Figure 6 shows ETG critical gradients for data in Figures 4 and 5. Figure 6 does not show ETG growth rates because ETG modes are linearly stable for the entire time period. The measurements indicate electron gyro-scale fluctuations are present during a period of ETG linear stability. Again, the observations are inconsistent with linear stability theory for ETG turbulence and suggest an additional turbulence mechanism is present.

III. TOROIDAL FIELD SCALING OF FLUCTUATION AMPLITUDES

H-mode confinement studies on NSTX indicate confinement improves at higher B_T largely due to reduced χ_e in the outer plasma, $r/a \gtrsim 0.5$ [18, 19]. The NSTX confinement time scaling for B_T is stronger than conventional tokamak scalings. Specifically, the NSTX energy confinement time scaling is $\tau_E \sim B_T^{0.85}$, but the ITER98PB,2 scaling is $\tau_E \sim B_T^{0.15}$. To investigate the B_T scaling of electron gyro-scale fluctuations, fluctuation measurements were obtained for H-mode discharges with 3.5, 4.5, and 5.5 kG toroidal fields [14].

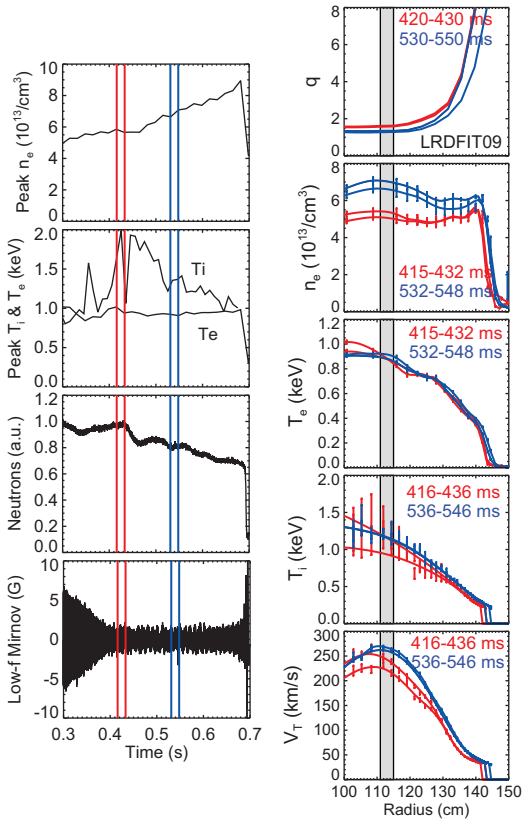

FIG. 4: Discharge 124885 with deuterium gas, $B_T = 5.5$ kG, $I_p = 700$ kA, and 4 MW of NBI heating. Fluctuation measurements were obtained at $R = 113 \pm 2$ cm (gray box).

Figure 7 shows profile quantities for 3.5, 4.5, and 5.5 kG discharges, and Figure 8 shows $E \times B$ shear rates, ETG linear growth rates, and fluctuation measurements. Discharge times were selected to best match electron temperature gradients, $E \times B$ shear rates, and ETG linear growth rates. Fluctuation amplitudes for the 3.5 kG discharge exceed amplitudes in the 4.5 kG discharge by more than 10 dB, but amplitudes in the 4.5 kG discharge are only about 5 dB greater than amplitudes in the 5.5 kG discharge. Note that $E \times B$ shear rates and ETG growth rates are similar for the 3.5 and 5.5 kG discharges, but the 4.5 kG discharge exhibits $E \times B$ shear rates noticeably greater than ETG growth rates. Accordingly, fluctuation amplitudes for the 4.5 kG discharge are expected to be disproportionately lower, as observed. Therefore, the measurements indicate fluctuation amplitudes decrease at higher B_T for similar plasma conditions. Note that the discharges in Figures 7 and 8 do not exhibit as strong a B_T dependence on confinement as the discharges in Refs. 18 and 19.

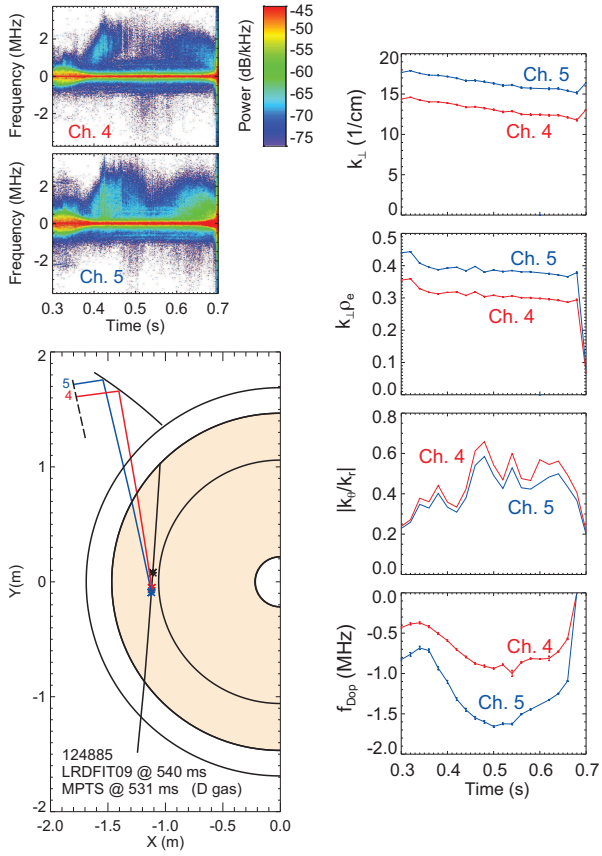

FIG. 5: Fluctuation measurements and ray tracing calculations for discharge 124885 at $R = 113 \pm 2$ cm in Figure 4.

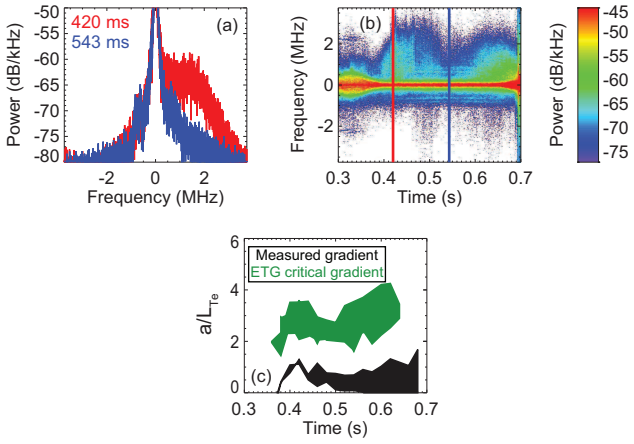

FIG. 6: (a and b) Fluctuation measurements for Ch. 5 and (c) electron temperature gradient and ETG linear critical gradient for data in Figures 4 and 5.

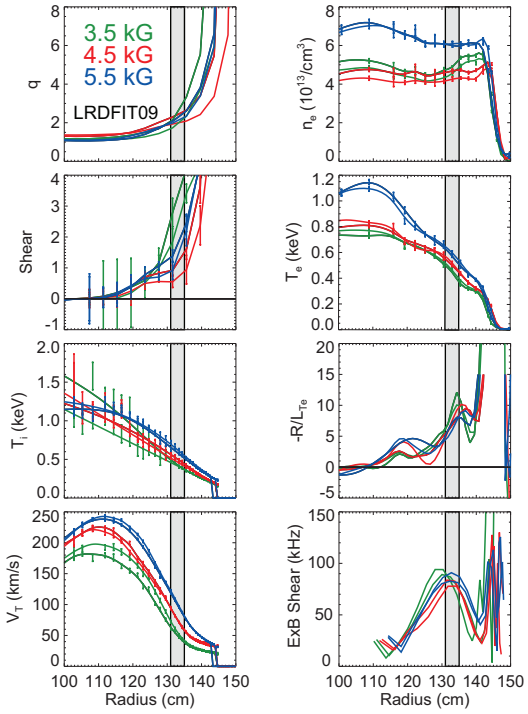

FIG. 7: Discharge profiles are shown for multiple discharges at $R = 133 \pm 2$ cm. The gray box marks the location of fluctuation measurements. (green) 124892 with $B_T = 3.5$ kG at 340 ms, (red) 124888 with $B_T = 4.5$ kG at 350 ms, and (blue) 124889 with $B_T = 5.5$ kG at 600 ms.

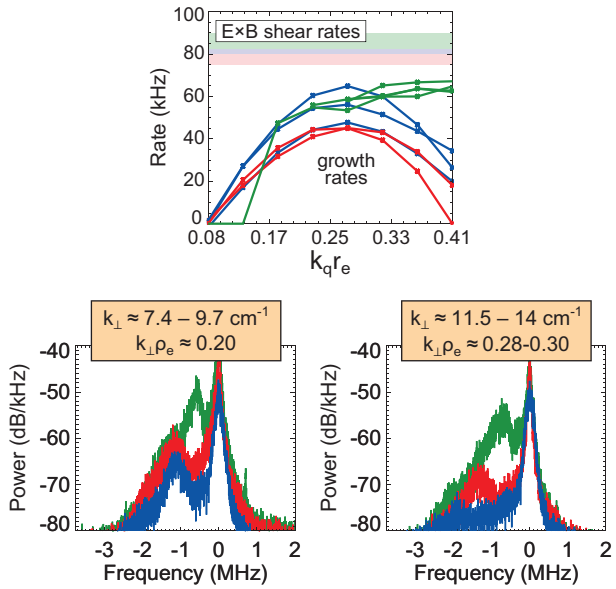

FIG. 8: $E \times B$ shear rates, ETG growth rates, and fluctuation measurements are shown for data in Figure 7. (green) 124892 with $B_T = 3.5$ kG at 340 ms, (red) 124888 with $B_T = 4.5$ kG at 350 ms, and (blue) 124889 with $B_T = 5.5$ kG at 600 ms.

IV. FLUCTUATIONS AND TRANSPORT

Feedback mechanisms complicate the relationship between fluctuations amplitudes and transport quantities. For example, if transport diffusivities increase and gradients decrease when fluctuation amplitudes increase, then the inference is that fluctuations induce transport. On the other hand, if fluctuation amplitudes increase when transport diffusivities decrease and gradients increase, then the inference is that fluctuations react to plasma conditions without inducing transport. Additionally, the relationship between turbulence and transport may depend critically upon the phase relation between fluctuations, marginal stability dynamics, or fluctuation correlation lengths. This Section presents fluctuation measurements and TRANSP calculations [20, 21] to investigate the relationship between electron gyro-scale fluctuation amplitudes and electron thermal transport [14].

Figure 9 shows fluctuation measurements and transport calculations at $R = 113 \pm 2$ cm and $r/a \approx 0.15$ for discharge 124887, a 4.5 kG H-mode discharge (see Figure 1). Recently, Global Alfven eigenmodes (GAEs) were proposed as a mechanism for anomalous electron thermal transport [22], so it is necessary to monitor GAE activity in Mirnov signals in the range 0.2–2 MHz. Figure 9 shows GAE activity is steady-state for 400–550 ms, so GAEs apparently can not account for changes in transport. Fluctuation amplitudes and the local temperature gradient increase from 400 to 550 ms. At the same time, the electron thermal diffusivity and electron heat conduction decrease. The observations suggest no simple relation exists between measured fluctuation amplitudes and electron thermal transport. A definitive assessment of the relationship between electron gyro-scale fluctuations and electron thermal transport requires simultaneous density and temperature fluctuation measurements.

Figure 10 shows fluctuation measurements and transport calculations at $R = 113 \pm 2$ cm and $r/a \approx 0.15$ for discharge 124885, a 5.5 kG H-mode discharge (see Figure 4). Again, GAE activity is steady-state for 550–650 ms, so GAEs apparently can not account for changes in transport. Fluctuation amplitudes increase from 550 to 650 ms while the temperature gradient remains unchanged. At the same time, the electron thermal diffusivity and electron heat conduction decrease. Again, the observations suggest no simple relation exists between measured fluctuation amplitudes and electron thermal transport.

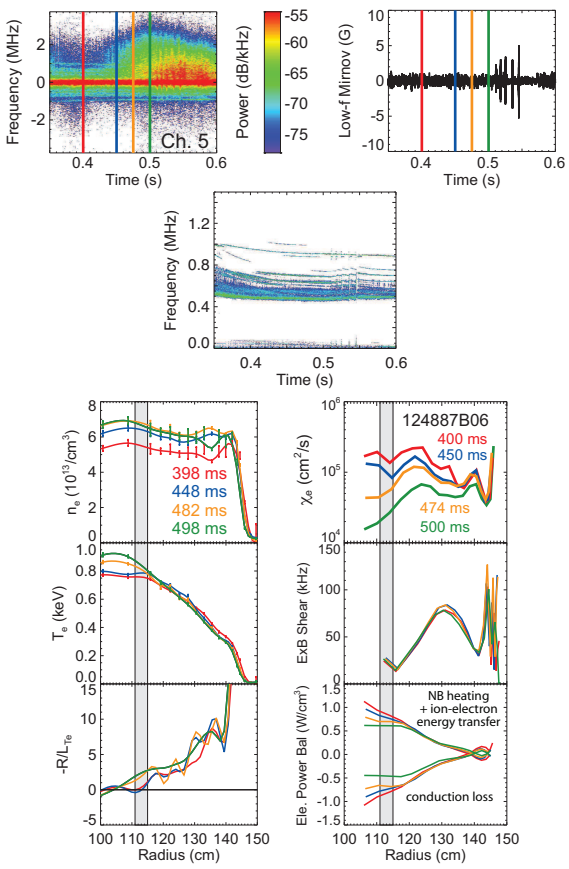

FIG. 9: Fluctuation measurements and transport calculations for discharge 124887 at $R = 113 \pm 2$ cm and $r/a \approx 0.15$

V. FLUCTUATION MAGNITUDES AND k-SPECTRA

Collective scattering measurements are inherently localized in k-space, whereas other fluctuation measurement techniques either employ a spatial array of probes or invoke a theoretical dispersion relation to attain k-space information (a notable exception is Doppler backscattering [23]). Linear gyrokinetic simulations provide linear growth rates and critical gradients, but nonlinear gyrokinetic simulations additionally provide fluctuation magnitudes and k-spectra. Fluctuation magnitudes and k-spectra from scattering measurements can be valuable validation tests for nonlinear gyrokinetic simulations. Accordingly, this Section presents fluctuation magnitudes and k-spectra from electron gyro-scale fluctuation measurements [14].

The k-space localization of scattering measurements is given by the k-matching condition $\boldsymbol{k_s} = \boldsymbol{k_i} \pm \boldsymbol{k}$ where $\boldsymbol{k_s}$ is the scattered wave vector, $\boldsymbol{k_i}$ is the incident wave vector, and $\boldsymbol{k}$ is

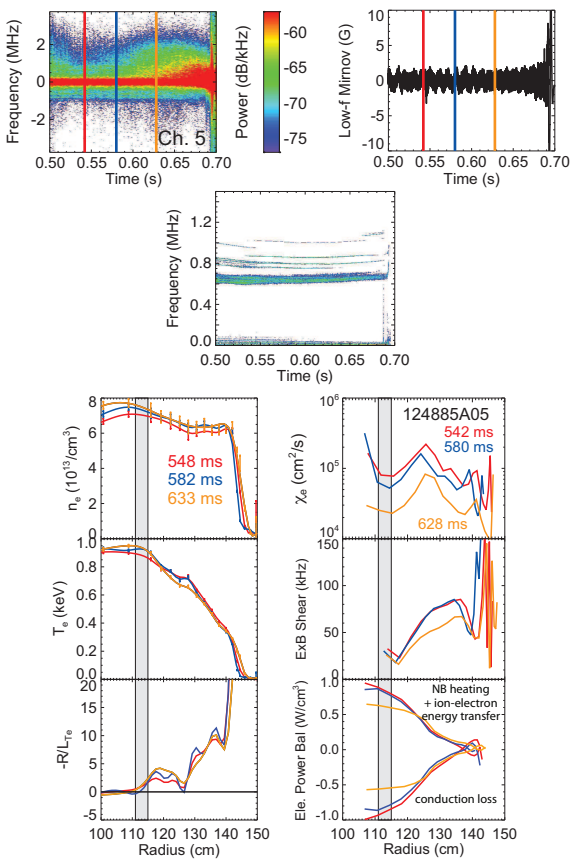

FIG. 10: Fluctuation measurements and transport calculations for discharge 124885 at $R = 113 \pm 2$ cm and $r/a \approx 0.15$

the measured fluctuation wave vector. The k-space resolution is $\Delta k = 2/a$. With $k_\parallel \approx 0$ ($k_\parallel$ is the component of $\boldsymbol{k}$ parallel to $\boldsymbol{B}$), scattering measurements are localized to an area $(\Delta k)^2$ in the k_θ-k_r plane. For a coherent density fluctuation with amplitude $\tilde{n}_e$, the total scattered power observed by a receiver with angular aperture $\pi(2/k_i a)^2$ is

$$P_s = \frac{1}{4} P_i \, r_e^2 \, L_z^2 \, \lambda_i^2 \, \tilde{n}_e^2. \tag{1}$$

where λ_i is the probe beam wavelength, $k_i = 2\pi/\lambda_i$ is the probe beam wave-number, a is the probe beam radius, P_i is the probe beam power, L_z is the length of the scattering volume, and r_e is the classical electron radius. Finally, the wavenumber spectral exponent α is defined such that $|\delta n_e(k)/n_e|^2 \propto k^{-\alpha}$.

Figure 11 shows discharges 124885 and 124889 at times with similar radial profiles. Both discharges have $B_T = 5.5$ kG, $I_p = 700$ kA, and 4 MW of NBI. Figure 12 shows fluctuation measurements at $R = 113 \pm 2$ cm in 124885 and at $R = 133 \pm 2$ cm in 124889. Multiple

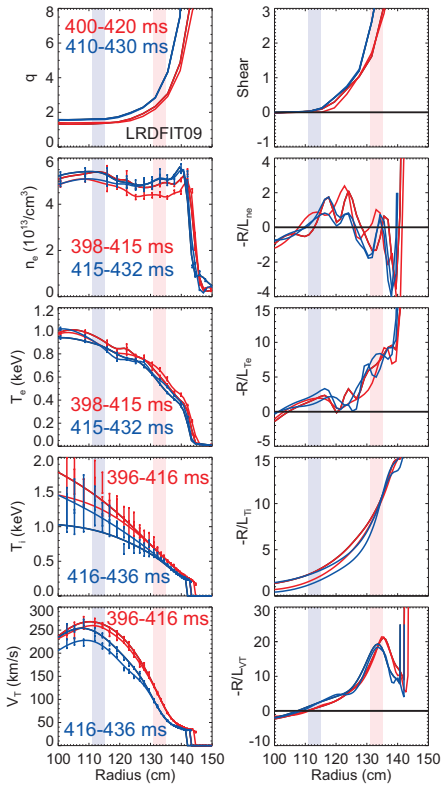

FIG. 11: Profile quantities and measurement locations for discharges 124885 (blue) and 124889 (red) are show.

detection channels provide k-spectra at both locations. At 133 cm the scattering volume lengths are 3–4 cm. On the other hand, at 113 cm the instrument selectivity function narrows to widths on the order of the probe beam wavelength. The location of the instrument selectivity peak varies by about 3 cm along the probe beam for rays within the probe beam antenna pattern, so the scattering volume length is assumed to be 3 cm. An accurate calculation of the scattering volume for measurement locations near the magnetic axis may require full-wave calculations. In Figure 12, the spectral exponent at $R = 133 \pm 2$ cm is $\alpha = 2.8$, and the spectral exponent at $R = 113 \pm 2$ cm is steeper with $\alpha = 4.6$. Additionally, fluctuation magnitudes are in the range $|\delta n_e(k)/n_e|^2 \approx 10^{-8}$–$10^{-9}$. The vertical error bars correspond to a ± 2 dB uncertainty in integrated spectral powers, and the horizontal error bars correspond to the k-space resolution, $\Delta k \approx 0.7$ cm^{-1}. Note that fluctuation measurements correspond to a k-space box with area $(\Delta k)^2$, not a k-space annulus in the k_θ-k_r plane. The spectral power uncertainty (± 2 dB) corresponds to a spectral exponent uncertainty $\Delta\alpha \approx 0.5$.

Nonlinear gyrokinetic simulations in Ref. 2 predict fluctuations magnitudes for typical

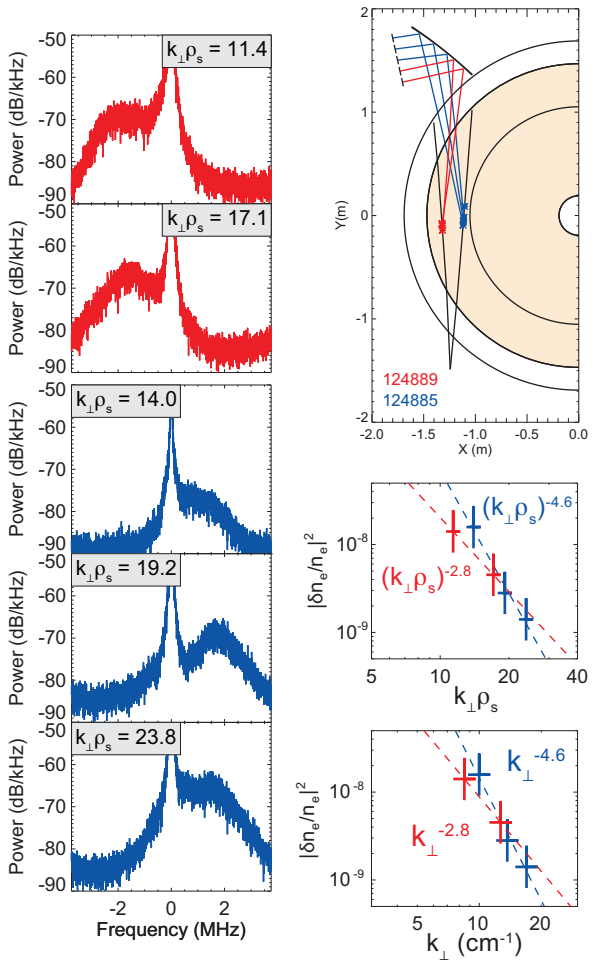

FIG. 12: Fluctuation magnitues and k-spectra for discharges 124885 (blue) and 124889 (red) in FIgure 11 are shown.

mid-radius tokamak parameters are $|\delta n_e/n_e|^2 \approx 10^{-11}$–$10^{-10}$ for $k_\perp \rho_s \approx$ 10–20 with k-space resolution $\Delta(k_\perp \rho_s) = 0.1$. On the other hand, fluctuation magnitudes in Figure 12 are $|\delta n_e/n_e|^2 \approx 10^{-9}$–$10^{-8}$ with k-space resolution $\Delta(k_\perp \rho_s) \approx$ 1–2. A direct comparison between fluctuation magnitudes in Figure 12 and Ref. 2 is not appropriate due to disparate plasma conditions, but it is nonetheless encouraging to note that the fluctuation magnitudes are within an order of magnitude when the k-space resolution is taken into account.

VI. SUMMARY

The NSTX collective scattering system has measured electron gyro-scale fluctuations to investigate ETG turbulence. Past measurements revealed electron gyro-scale fluctuations

in NSTX L-mode plasmas with high-harmonic fast-wave heating [11, 12]. Enhanced fluctuations were observed when the local electron temperature gradient exceeded the ETG linear critical gradient, and the enhanced fluctuations propagated with a component in the electron diamagnetic direction. In NSTX H-mode plasmas with NBI heating, past measurements revealed electron gyro-scale fluctuations when the electron temperature gradient was marginally stable with respect to the ETG linear critical gradient, and fluctuation amplitudes decreased when the equilibrium $E \times B$ shear rate exceeded ETG linear growth rates [13]. This Paper has presented observations and results covering several additional topics [14]. Electron gyro-scale fluctuations were observed in an ETG-stable region near the magnetic axis in H-mode plasmas. Fluctuation amplitudes decrease at higher toroidal field in plasma regimes with similar electron temperature gradients, $E \times B$ shear rates, and ETG linear growth rates. Transport analysis revealed instances in which the electron thermal diffusivity decreased when measured fluctuation amplitudes increased, which suggests no simple relation exists between measured fluctuation amplitudes and electron thermal transport. Wavenumber spectral exponents are in the range 2.8–4.6 for H-mode plasmas, and fluctuation magnitudes are $|\delta n_e(k)/n_e|^2 \approx 10^{-9}$–$10^{-8}$. Finally, fluctuation magnitudes are within an order of magnitude of nonlinear gyrokinetic simulations for mid-radius tokamak parameters [2] when the k-space resolution is taken into account.

Acknowledgments

This work was supported by the U. S. Department of Energy under Contract Nos. DE-AC02-76CH03073, DE-FG03-95ER54295, and DE-FG03-99ER54518.

[1] W. M. Nevins et al., Phys. Plasmas **13**, 122306 (2006).

[2] R. E. Waltz, J. Candy, and M. Fahey, Phys. Plasmas **14**, 056116 (2007).

[3] W. Dorland et al., Phys. Rev. Let. **85**, 5579 (2000).

[4] F. Jenko et al., Phys. Plasmas **7**, 1904 (2000).

[5] F. Jenko and W. Dorland, Phys. Rev. Let. **89**, 225001 (2002).

[6] M. Ono et al., Nucl. Fusion **40**, 557 (2000).

[7] S. M. Kaye et al., Phys. Plasmas **8**, 1977 (2001).

[8] D. R. Smith et al., Rev. Sci. Instrum. **75**, 3840 (2004).

[9] W. Lee et al., Rev. Sci. Instrum. **79**, 10E723 (2008).

[10] D. R. Smith et al., Rev. Sci. Instrum. **79**, 123501 (2008).

[11] E. Mazzucato et al., Phys. Rev. Let. **101**, 075001 (2008).

[12] E. Mazzucato et al., Nucl. Fusion **9**, 055001 (2009).

[13] D. R. Smith et al., Phys. Rev. Let. **102**, 225005 (2009).

[14] D. R. Smith (2009), Ph.D. Dissertation, Princeton University.

[15] E. Mazzucato, Phys. Plasmas **10**, 753 (2003).

[16] E. Mazzucato, Plasma Phys. Control. Fusion **48**, 1749 (2006).

[17] K. L. Wong et al., Phys. Rev. Let. **99**, 135003 (2007).

[18] S. M. Kaye et al., Nucl. Fusion **47**, 499 (2007).

[19] S. M. Kaye et al., Phys. Rev. Let. **98**, 175002 (2007).

[20] R. J. Goldston et al., J. Comp. Phys. **43**, 61 (1981).

[21] R. J. Hawryluk, in *Physics of Plasma Close to Thermonuclear Conditions* (1980).

[22] D. Stutman et al., Phys. Rev. Let. **102**, 115002 (2009).

[23] L. Schmitz et al., Rev. Sci. Instrum. **79**, 10F113 (2008).

The Princeton Plasma Physics Laboratory is operated
by Princeton University under contract
with the U.S. Department of Energy.

Information Services
Princeton Plasma Physics Laboratory
P.O. Box 451
Princeton, NJ 08543

Phone: 609-243-2750
Fax: 609-243-2751
e-mail: pppl_info@pppl.gov
Internet Address: http://www.pppl.gov